Energy transfer during resonant neutralization of hyperthermal protons at an aluminum surface studied with time-dependent density functional theory

Lukas Deuchler* and Eckhard Pehlke†
Institut für Theoretische Physik und Astrophysik, Christian-Albrechts-Universität zu Kiel, D-24098 Kiel, Germany

(Received 20 August 2020; accepted 1 December 2020; published 17 December 2020)

We present time-dependent density functional molecular dynamics (TDDFT-MD) simulations with an adiabatic approximation to the exchange-correlation potential for hyperthermal protons (H^+) with initial kinetic energies in the range of 2–50 eV impinging on the fcc-hollow site and the on-top site of an Al(111) surface. The surface is modeled by a finite-size cluster and the results are generalized to H^+-Al surface scattering. From the simulation, neutralization distances are determined and the time development of the kinetic energy and the electronic excitation energy are derived. The results can be rationalized on the basis of the ground-state potential energy surface and the H^+-Al(111) interaction potential. Furthermore, the difference in initial kinetic energy between H^+ and H^0 projectiles required to yield identical exit velocities is derived. Notably, this difference changes sign within the studied range of kinetic energies. This is traced back to the neutralization distances and the difference between both the ground-state potential energy surface and the H^+-Al(111) interaction potential at those distances.

DOI: 10.1103/PhysRevB.102.235421

I. INTRODUCTION

Modeling the interaction of plasmas with solid surfaces is a challenging problem within low-temperature plasma science and technology [1,2]. Ions are accelerated by the plasma sheath potential and can be scattered, and neutralized, at the surface. The question of charge transfer dynamics in ion scattering has often been approached from the theoretical side by using a Brako-Newns-Anderson type Hamiltonian [3–5] or an LCAO Hamiltonian [6]. There also exist approaches based on a Newns-Anderson Hamiltonian that describe correlation with the help of Green's function techniques [7–9]. In this paper we will discuss results from time-dependent density functional theory (TDDFT) simulations [10–12] for the charge and the energy transfer during the collision of a hyperthermal ion (i.e., an ion with an initial kinetic energy in the sub-eV up to few 10-eV range) with a metal surface. In these simulations, the entire information about the electronic structure of the projectile and the substrate is taken into account. As an example already intensely investigated experimentally [13–21] and theoretically [6,22–34] by various groups, we consider a proton (H^+ ion) incident on an Al(111) surface. The main focus of our study will be on the energy transfer from the incident ion into the electronic degrees of freedom of the substrate.

In his review, comparing the scattering of neutral projectiles and ionic projectiles which are or are not neutralized, Winter [15] traces back energy and angle shifts observed in the spectra of the projectile after scattering at the metal surface to an image charge effect. As he points out, this effect should provide a means to experimentally estimate the neutralization distance of the H^+ projectile by observation of the kinetic energy transfer: The acceleration and deceleration of the projectile by the attractive force from its image charge—as long as it is not neutralized—affects the kinetic energy and angle distribution of the scattered (neutralized) particle. However, Winter also explicates that for H^+ scattered at an Al(111) target the experimental data suggest a peak of the distribution function of charge transfer at around 6 bohr in front of the image plane, while the value expected from theory was around 3 bohr [15,35]. It has been argued that Auger neutralization should dominate over the resonant charge transfer process in order to understand the experiment [16]. Merino *et al.* [25], however, have come to the conclusion that at low proton kinetic energies (less than 4 keV) the charge transfer between the Al orbitals and the hydrogen 1s orbital is a resonant one. Moreover, in Ref. [6] Merino *et al.* construct a "diabatic" state and present an interaction energy of the proton (H^+) in front of an Al(100) surface, which deviates from the $1/[4(z - z_{\text{image}})]$ image behavior when the proton gets close to the surface. In this paper we present TDDFT molecular dynamics (MD) simulations for the resonant charge transfer of hyperthermal protons incident on an Al(111) surface. As we deal with small kinetic energy of the projectile we do not consider further effects like core electron promotion [36]. We demonstrate a method to derive an approximation to the H^+-Al(111) interaction potential directly from the simulation by means of an extra TDDFT-MD run for a fast (1 keV) proton. This yields the "generalization" of the image potential to small (<7 bohr) projectile–surface separations, where the interaction indeed becomes repulsive. This affects the energy transfer between the projectile and the metal.

*deuchler@theo-physik.uni-kiel.de
†pehlke@theo-physik.uni-kiel.de

 ©2020 American Physical Society

II. COMPUTATIONAL METHODS

The simulations (i.e., both the TDDFT-MD simulations and the DFT-based relaxations) have been carried through with the program OCTOPUS (version 6) [12,37,38]. The generalized gradient approximation PBE-GGA [39] has been used for the exchange-correlation energy functional (from ground-state DFT). The H^+ ion is incident normally to an Al(111) surface at a fcc-hollow or a top site. The surface is modeled using Al clusters with 172 or 188 atoms for H^+ incident at the fcc-hollow or top site, respectively. The clusters have been created starting from a relaxed Al(111) surface (with a theoretical Al lattice constant 7.648 bohr) and cutting out a half sphere. Subsequently, the uppermost layer of Al atoms has been kept fixed and the cluster has been relaxed ionically until the forces are below 10^{-3} Hartree/bohr. H and Al are described by ionic semilocal norm-conserving Troullier-Martins pseudopotentials [40] created and analyzed using the FHI98PP software [41]. The Al pseudopotential has been created with 10 electrons as frozen-in core states and cutoff radii $r_s^{Al} = 1.791$ bohr, $r_p^{Al} = 1.974$ bohr, $r_d^{Al} = 2.124$ bohr. The p potential has been chosen as the local potential. For the H pseudopotential we have used cutoff radii $r_s^H = r_p^H = 1.276$ bohr, and the s potential has been chosen as the local potential.

In the time-dependent simulations, the adiabatic approximation is applied to the exchange-correlation (XC) potential v_{XC}, together with the above mentioned PBE-GGA [39] for the XC functional from ground-state DFT. The wave functions are confined to a user-defined box with distance between the box edge and atoms of at least 12 bohr, which fits into a cube with 60-bohr edge length. The FFT for solving the Poisson equation requires a box with twice the edge length of this cube. A Coulomb kernel with a spherical cutoff as provided within OCTOPUS has been used [42]. The Kohn-Sham wave functions are sampled on a real-space mesh with mesh spacing $\Delta x = 0.5$ bohr. The filtering method of Tafipolsky and Schmid [43] is applied to the pseudopotentials in order to avoid Fourier components above the cutoff determined by the mesh spacing. Prior to the time-dependent simulation, the electronic ground state of the Al cluster was determined. Formally, a Methfessel-Paxton smearing [44] has been applied, with the smearing parameter finally reduced to the very small value of 20 meV.

The time-dependent Kohn-Sham wave functions are propagated using a time step of 0.02 atu (0.5 attoseconds). For simplicity, the ionic time step has been chosen identical to the electronic time step. After the ground state of the Al cluster has been determined, a bare H pseudopotential has been added to the simulation box at a distance of 16 bohr above the first layer of Al-surface atoms. The total charge of the system is +1 (i.e., equals the proton charge). In order to minimize the number of ground-state calculations for the subsequent determination of electronic excitation energies, all Al atomic coordinates are kept frozen during the time-dependent simulations. The only exceptions are three simulations entering Table II, which, beside electronically nonadiabatic effects, include the kinetic energy transfer into the substrate ionic degrees of freedom (13 Al atoms were allowed to move). In those simulations, the position of the ions follows from Ehrenfest dynamics [12,45], i.e., the ions move along a unique trajectory.

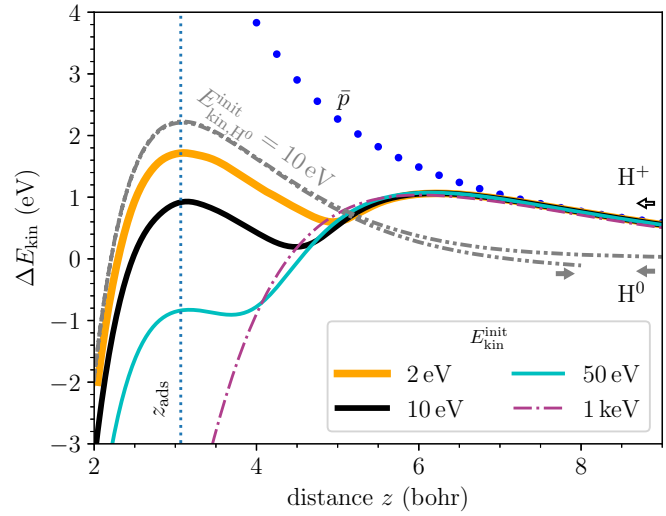

FIG. 1. Variation of kinetic energy for protons (H^+, solid and dash-dotted curves) and a spin-unpolarized hydrogen atom (H^0, dash-dot-dotted curve) impinging on the Al(111) on-top site of an Al_{188} cluster. For comparison, the change of ground-state potential energy for an antiproton is shown ($\bar{p}$, dots). The initial kinetic energy of the projectile at $z_{init} = 16$ bohr is noted in the legend.

For convergence analysis, time-dependent calculations for the $E_{kin}^{init} = 10$ eV on-top trajectory have been performed with a larger Al-cluster size of 302 atoms. As a result, the values for charges $q(z)$ as defined in Eq. (4) vary less than $0.03e$. Decreasing either the mesh spacing Δx from 0.5 to 0.4 bohr, or the time step Δt from 0.02 to 0.01 atu resulted in a variation of q that is one order of magnitude less. Regarding the kinetic energy convergence with Δx and Δt, maximum differences of 10 meV were obtained during scattering, in both cases.

Regarding the accuracy of the dissipated energy, we compared the kinetic energy loss of an H^0 atom impinging on the Al(111) fcc-hollow site of an Al_{52} and an Al_{172} cluster with $E_{kin}^{init} = 10$ eV. The difference due to the two cluster sizes amounts to 200 meV with respect to the propagation inside the bulk from $z^{in} = 8$ bohr to $z^{out} = 8$ bohr with reflection at the third layer. For comparison, in this case a total energy of 3.0 eV is dissipated due to electronic friction effects.

III. RESULTS

A. Proton impinging on Al(111) on-top site

We have carried through TDDFT-MD simulations for H^+ ions starting at $z_{init} = 16$ bohr in front of the Al cluster with initial kinetic energy E_{kin}^{init} of 2, 10, and 50 eV. The proton is incident normally to the Al(111) surface at the on-top position. The change of kinetic energy of the projectile,

$$\Delta E_{kin} = E_{kin}(z(t)) - E_{kin}^{init}, \tag{1}$$

is shown in Fig. 1 as a function of distance z of the H^+ from the topmost Al layer. We find that—as long as the electron transfer from the cluster to the H^+ has not yet occurred—all curves almost lie on top of each other, independent of the initial kinetic energy. This is interpreted in terms of conservation

of total energy $E_{\rm kin}(z) + E_{\rm tot}^{(+)}(z)$. Here $E_{\rm tot}^{(+)}(z)$ denotes the (non-ground-state) potential energy of a positive elementary charge in front of the electrically polarized cluster, provided that there is no charge transfer (i.e., describing the interaction of the positive charge with its induced image dipole). In order to obtain an estimate for this H^+-Al(111) interaction potential $E_{\rm tot}^{(+)}(z)$ in Fig. 1 we present the change of kinetic energy $\Delta E_{\rm kin}$ of a fast H^+ projectile with initial kinetic energy equal to 1 keV. From the projection of the time-dependent Kohn-Sham orbitals onto the H1s orbital (details will be given below) we conclude that the charge transfer to the 1-keV projectile is negligible (less than 0.05 $|e|$) as long as $z > 4.5$ bohr.

B. H^+-Al(111) interaction potential

Our simple interpretation of the motion of the H^+ in terms of a potential energy surface $E_{\rm tot}^{(+)}(z)$ neglects energy dissipation due to dynamical screening [46,47] of the Coulomb potential of the positively charged projectile incident on the metal surface. In order to obtain a rough estimate for the electronically nonadiabatic effects due to the electron-hole pair excitations in the Al cluster induced by coupling to the time-dependent Coulomb potential of the projectile we have carried through TDDFT-MD simulations for antiprotons with initial kinetic energy 50 eV, 1 keV, and 10 keV. The initial configuration has been prepared by adding the antiproton to a simulation box containing an uncharged, electronically relaxed Al cluster. We note that therewith the polarization of the Al cluster by the antiproton has been neglected in the initial state deliberately (in order to stay in line with the H^+ simulations). The contribution of the antiproton at $\mathbf{r}_{\bar{p}}$ to the electron potential energy is described by a soft Coulomb potential,

$$v_{\bar{p}}(\mathbf{r}) = \frac{1}{\sqrt{(0.2\,\text{bohr})^2 + |\mathbf{r} - \mathbf{r}_{\bar{p}}|^2}}. \tag{2}$$

Results are summarized in Fig. 2 and compared to the variation $\Delta E_{\rm kin}$ obtained from energy conservation and the Born-Oppenheimer surface of the antiproton in front of the metal cluster. Even up to $E_{\rm kin}^{\rm init} = 1$ keV the energy dissipation stays small on the energy scale shown, i.e., 80 meV at $z = 5$ bohr and 150 meV at $z = 4$ bohr. For a comparison of results for H^+ approaching a jellium surface we refer the reader to Ref. [48]. In case of the faster antiproton with initial kinetic energy of 10 keV, the electronically nonadiabatic effects become distinctly larger, as can be read from Fig. 2. Hence such a simulation would not be useful any more for our purpose of approximating a quasiadiabatic potential energy surface—while the 1-keV result appears to be useful in the sense that electronically nonadiabatic effects stay sufficiently small. For this reason we still use 1-keV trajectories for comparison in case of H^+ incident on the Al surface.

In Fig. 1 $\Delta E_{\rm kin}$ derived from the Born-Oppenheimer surface of the antiproton is compared to $\Delta E_{\rm kin}$ for H^+ incident on the (111) surface of an Al cluster with initial kinetic energy of 1 keV. At large distance, $z > 7$ bohr, the two curves for $\Delta E_{\rm kin}$ nearly coincide. At smaller H^+-cluster separation the (approximate) potential energy of the positively charged H^+ and the negatively charged $\bar{p}$ projectiles start to deviate strongly from each other. This cannot be ascribed to an electronically nonadiabatic effect, as the energy dissipation for the antiproton has been shown to be small and the respective difference persists also for small kinetic energy of the H^+. Obviously, the electric polarization of the Al cluster can no longer be described within linear response. The H^+ projectile is decelerated which we attribute to the Coulomb repulsion between the H^+ and the Al ion cores. This means that even before neutralization the dynamics of the H^+ does not follow the simple $1/[4(z - z_{\rm image})]$ image potential, but that $E_{\rm tot}^{(+)}(z)$ becomes repulsive at short distance to the Al metal surface. We emphasize that there is an analogous result already known in the literature: Merino *et al.* [25] have constructed a "diabatic" state and obtained an interaction energy of H^+ in front of an Al(100) surface that deviates from the image potential in a similar way.

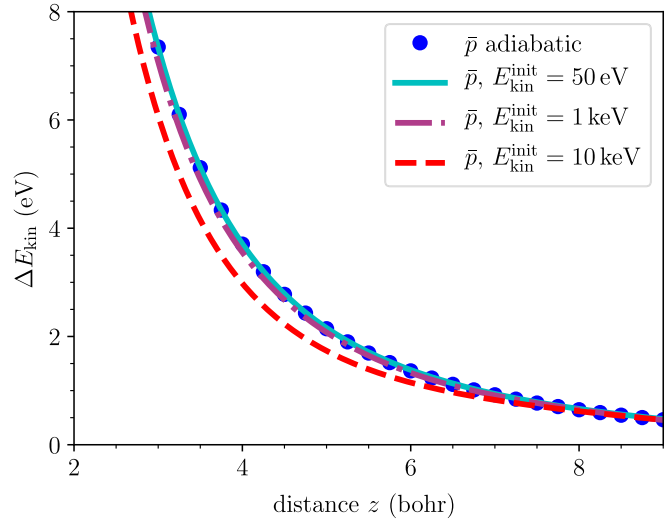

FIG. 2. Variation of the kinetic energy of an antiproton ($\bar{p}$) incident normally on the Al(111) surface of the Al_{188} cluster at the Al on-top site for initial kinetic energy at $z_{\rm init} = 16$ bohr of 50 eV, 1 keV, and 10 keV. Initially, the antiproton has been positioned in front of the not electrically polarized Al cluster. Data are compared to $\Delta E_{\rm kin}(z)$ derived from energy conservation and the Born-Oppenheimer surface of an antiproton in front of the Al cluster.

C. Comparison of trajectories between initially neutral and charged cluster

In order to exclude artifacts in the simulation due to the charging of the Al cluster during H^+ neutralization we have performed a simulation with a proton incident on an initially negatively charged Al_{188}^- cluster. The comparison to a simulation for H^+ incident on the initially neutral Al_{188}^0 cluster is shown in Fig. 3. Due to the stronger Coulomb attraction between H^+ and Al_{188}^-, the projectile is accelerated more strongly while approaching the surface. We have accounted for this extra acceleration by choosing a smaller initial kinetic energy of 9.7 eV of the proton in case of H^+ incident on Al_{188}^-. This is consistent with the difference in potential energy of an antiproton in front of an Al_{188}^0 cluster or an Al_{188}^- cluster at distances $z = 8$ bohr and $z = 16$ bohr. As can be read from Fig. 3, the kinetic energy as a function of the z coordinate in case of both trajectories of the H^+-Al_{188} cluster basically

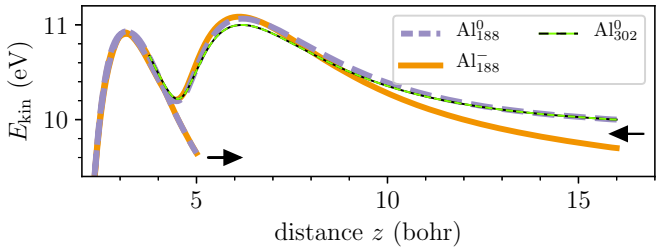

FIG. 3. Kinetic energy of a proton with $E^{init}_{kin} = 10\,eV$ at $z_{init} = 16\,bohr$ (dashed lines) and $E^{init}_{kin} = 9.7\,eV$ (solid line) impinging at the top site of a neutral Al^0_{188} (thick dashed line), a neutral Al^0_{302} (thin dashed line), or a negatively charged Al^-_{188} cluster (thick solid line).

coincides for separations less than about 8 bohr. The similarity of the variation of E_{kin} vs z for $z < 8$ bohr in case of the Al_{188} simulations shown in Fig. 3 suggests that at a separation of the H^+ projectile from the infinitely extended Al(111) surface less than about 8 bohr the projectile-surface interaction can be approximated by the TDDFT-MD cluster simulation. We argue that the difference between the screening charges for the charged and uncharged cluster will be more extreme than the difference between the screening charges induced in the uncharged cluster and the infinitely extended surface. To investigate this in more detail, a simulation with a neutral cluster containing 302 Al atoms is also shown in Fig. 3. For H-Al distances <8 bohr,

$$\left|\left(E^{Al_{302}}_{kin}(z) - E^{Al_{302}}_{kin}(z = 8\,bohr)\right) - \left(E^{Al_{188}}_{kin}(z) - E^{Al_{188}}_{kin}(z = 8\,bohr)\right)\right| < 0.1\,eV. \quad (3)$$

In the following we shall use the results of the Al-cluster simulations for H-Al distances <8 bohr to describe interaction between H^+ and the infinitely extended Al(111) surface.

D. Electronic energy transfer in the neutralization region for impact at on-top and fcc-hollow site

When the H^+ projectile approaches the surface, charge is transferred from the Al cluster to the projectile at some separation which depends on E^{init}_{kin}. The electronic charge q at the projectile has been derived by a projection of the time-dependent Kohn-Sham wave functions $\psi_j(t)$ onto the hydrogen 1s orbital ϕ^{H1s}, i.e.:

$$q(t) = \sum_j^{occ} |\langle \psi_j(t) | \phi^{H1s}(z(t)) \rangle|^2. \quad (4)$$

Spin degeneracy is accounted for by twofold occurrence of wave functions in the summation. The charge calculated in this way is quantitatively consistent with a Bader charge analysis [49] of the electron density. Figure 4 shows the charge transfer rate dq/dz from the surface towards the projectile impinging on the Al(111)-top site. dq/dz shows an extremum at 5.13, 4.76, and 4.18 bohr in case of $E^{init}_{kin} = 2$, 10, and 50 eV, respectively. Within the TDDFT-MD approach, the charge transfer region is broad. The charge $q(z)$ is not normalized; it approaches values distinctly larger than one in case of the H atom getting close to (and hence chemically interacting with) the Al surface. Hence we refrain from an interpretation of dq/dz in terms of a transition probability.

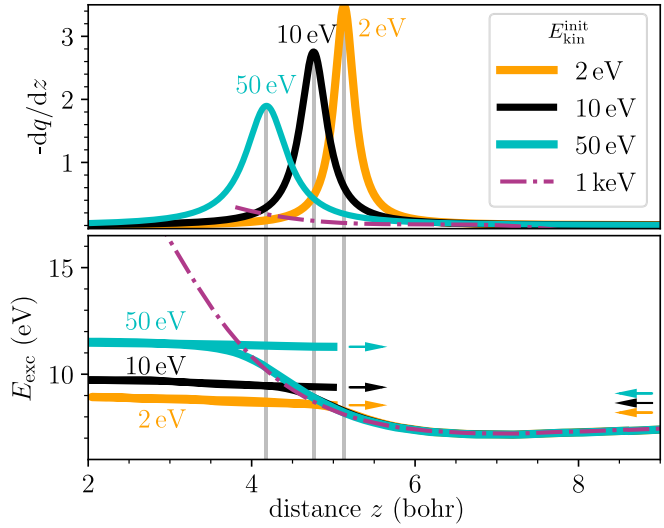

FIG. 4. H^+ impinging on the (111) facet of the Al cluster at the on-top position. (Top) $-dq/dz$, with q denoting the electronic charge on the projectile and z the projectile-surface distance for H^+ projectiles with $E^{init}_{kin} = 50$, 10, and 2 eV. Units are |e|/bohr. Charges have been calculated using Eq. (4). (Bottom) Excitation energy as defined in Eq. (5).

The electronic excitation energy E_{exc} of the complete system (including the hydrogen projectile and the Al cluster) is defined by the difference between the electronic energy E_{elec} from the time-dependent (TD) simulation and the electronic energy of the system in its electronic ground state (BO):

$$E_{exc}\left(z(t), E^{init}_{kin}\right) := E^{TD}_{elec}\left(z(t), E^{init}_{kin}\right) - E^{BO}_{elec}(z(t)). \quad (5)$$

Results are shown in the bottom panel of Fig. 4. For illustration we note that in case of an extended (periodic) metal surface and initially infinite proton-surface separation the excitation energy E_{exc} would correspond to the ionization energy of the projectile (13.6 eV) minus the surface work function [4.09 eV in case of Al(111)[50]].

Next we address the dependence of excitation energy on the impact site. As our focus is on electronic excitations, we still keep the atom coordinates of the Al substrate frozen. The H^+ has been chosen to impinge on the fcc-hollow site of the Al(111) surface, as distinct differences to impact onto the Al top site are to be expected in this case. Simulation results are summarized in Fig. 5. The charge transfer $-dq/dz$ is virtually identical for impact on fcc-hollow and top sites. As to be expected, the energy dissipation is distinctly larger for the H^+ incident on the Al-hollow site as (after neutralization) the projectile penetrates into the Al substrate and experiences energy losses by electronic friction [51,52].

As motivated above, as a reference for the excited system we choose E_{exc} from the 1-keV trajectory (this system has almost negligible charge transfer within the range of z in Fig. 4; see Sec. III A). In fact, the E_{exc} curves for $E^{init}_{kin} = 2$, 10, and 50 eV—where E^{init}_{kin} is the kinetic energy of the proton at $z = 16\,bohr$—closely overlap with this reference as long as the charge transfer is negligible. When the charge transfer is almost completed, the excitation energy stops following E^{1keV}_{exc} and—in case of the impact at the on-top site—does not vary more than 100 meV over the remaining trajectory. We obtain

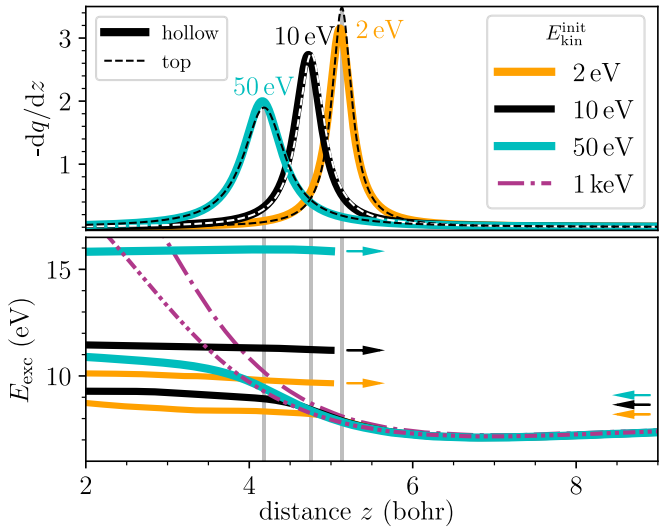

FIG. 5. H^+ impinging on the (111) facet of the Al cluster at the fcc-hollow position. (Top) Same quantity as in Fig. 4 but for the fcc-hollow impact point. For comparison, data for impact at the on-top site are shown by dashed lines. (Bottom) Excitation energy as defined in Eq. (5). Dash-dotted line represents the $E_{\rm kin} = 1$ keV trajectory with impact point at the on-top site.

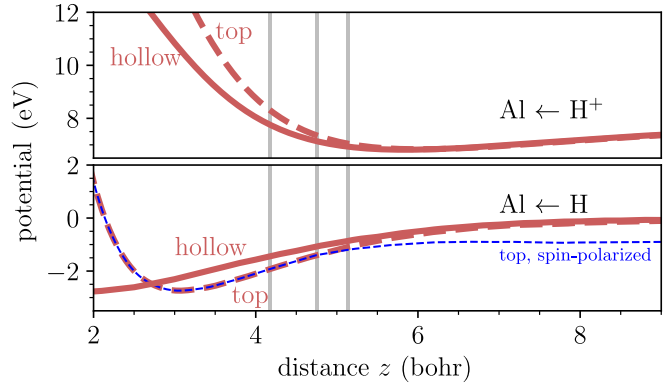

FIG. 6. Born-Oppenheimer surface of the spin-unpolarized H-Al cluster system with total charge +1 (lower graph) and interaction potential curve of an H^+ projectile with $E_{\rm kin}^{\rm init} = 1$ keV (proton in front of the cluster, upper graph). Thick full lines denote results for impact at the fcc-hollow site, and thick dashed lines denote results for impact at the on-top site. For comparison, the Born-Oppenheimer surface of an H^0 in front of the Al_{188} cluster from a calculation that allows for spin polarization is also shown (thin blue dashed curve). Vertical lines mark the extrema of dq/dz from Fig. 4.

$E_{\rm exc} = 8.6\,{\rm eV}/9.4\,{\rm eV}/11.3\,{\rm eV}$ for $E_{\rm kin}^{\rm init} = 2$ eV, 10 eV, and 50 eV, respectively, at $z = 5$ bohr on the outgoing trajectory.

In case of impact at the fcc-hollow site (see Fig. 5), a direct analysis of the data is complicated by the additional strong electronic friction that arises during propagation of the H through the bulk material. We will target this issue in the following section.

The charge of the outgoing particle (while not well described within spin-unpolarized DFT—the ionicity comes out too negative) is close to the charge calculated for the respective ground state. Hence the simulated ionicity of the scattered projectile is not an indication for a true excitation of the outgoing particle, and we suggest that the excitation energy is finally mostly deposited in the electronic degrees of freedom of the target. In case of the on-top trajectory it can be read from Fig. 4.

E. Energy dissipation after neutralization and comparison to neutral hydrogen

The total energy $E_{\rm BO}$ (i.e., the potential energy) for a hydrogen atom H^0 in front of the on-top and fcc-hollow sites of an Al cluster is visualized in the bottom panel of Fig. 6. In case of the H atom kept fixed atop the Al on-top position, the energy minimum of the one-dimensional cut through the potential energy surface is at $z = 3.1$ bohr. It is a well-known property of currently feasible approximations to the ground-state XC functional, that the electronic ground state of an H^0 atom far away from the surface has to be taken from a spin-polarized calculation. At distances smaller than about 5 bohr, the electronic ground states from a spin-unpolarized and a spin-polarized calculation coincide, in agreement with Ref. [53]. Thus, in case of a proton incident on the Al surface, for the incoming part of the trajectory spin polarization is not expected to be relevant because neutralization mostly takes place at a H-Al separation where the energy difference between spin-polarized and spin-unpolarized ground state is small. However, for a neutral particle moving away from the surface, the energy difference between a spin-polarized and a spin-unpolarized simulation would affect the kinetic energy of the outgoing projectile. Due to this inherent property of the chosen approximate XC functional we show results only for distances up to 5 bohr in the exit trajectory. The upper curves of Fig. 6 represent a H^+-Al(111) interaction potential, i.e., H^+ in front of the Al cluster. The curve is calculated from the electronic and ionic energy of the simulation with the $E_{\rm kin} = 1$ keV H^+ projectile.

In order to separate the electronic friction effects after neutralization from effects due to H^+ propagation and neutralization one has to subtract the excitation energy of an H^0 projectile from the $E_{\rm exc}$ of H^+:

$$\Delta E_{\rm exc}(z) := E_{\rm exc}\left(z, E_{\rm kin}^{\rm init}\right) - E_{\rm exc}^{\rm H^0}\left(z, E_{\rm kin}^{\rm init,H^0}\right). \qquad (6)$$

$E_{\rm kin}^{\rm init,H^0}$ should be chosen in such a way that kinetic energies between H^+ and H^0 coincide after the charge transfer. For simplicity, we have chosen $E_{\rm kin}^{\rm init,H^0} = E_{\rm kin}^{\rm H^+}(z = 16\,{\rm bohr})$. This leads to a difference in $E_{\rm kin}$ after charge transfer between the H^0 and H^+ trajectories of about 0.4, 0.7, and 1.6 eV (for $E_{\rm kin}^{\rm init,H^0} = 2$, 10, and 50 eV).

For the results shown in Fig. 7 we have treated the scattering of the H^0 at the Al cluster also spin unpolarized. The resulting $\Delta E_{\rm exc}$ for $E_{\rm kin}^{\rm init} = 2$, 10, and 50 eV are shown as full lines in the panels of Fig. 7. They are compared to respective results for impact on the Al(111) top site (dashed lines). Note that the difference in $\Delta E_{\rm exc}$ arises not only because the ground-state potential energy of H adsorbing atop the Al on-top or fcc-hollow site for the same distance is different, but also because the H^+-Al(111) interaction potential for both situations is differently corrugated, too, as can be seen in Fig. 6. $\Delta E_{\rm exc}$ is determined by that part of the trajectory before

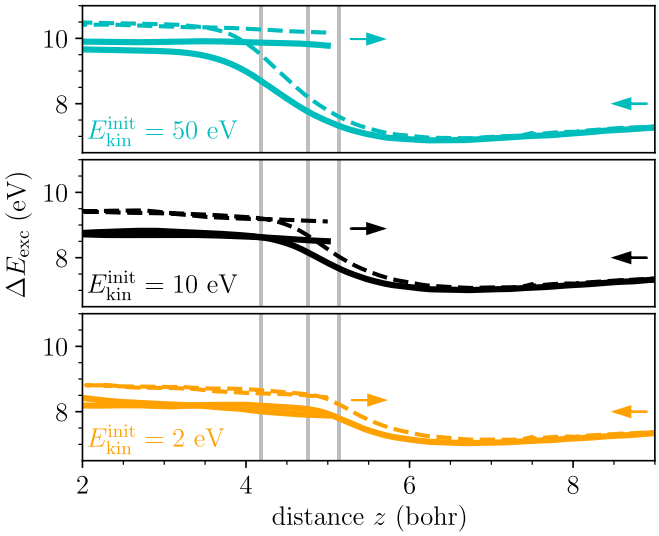

FIG. 7. Difference of the electronic excitation energy between an H^+ impinging on an Al cluster and an H^0 impinging on an Al cluster. $\Delta E_{\rm exc}$ is defined in Eq. (6); here the kinetic energies of H^+ and H^0 are chosen to coincide at $z = 16$ bohr and are denoted in the inset of the graphs. The simulation for the H^+ as well as for the H^0 was treated spin unpolarized. For comparison, two different impact sites are shown: on-top (dashed lines) and fcc-hollow (straight lines) sites. Arrows denote the direction of motion.

neutralization where the projectile moves in the generalized image potential. The difference in $\Delta E_{\rm exc}$ at $z_{\rm exit} = 5$ bohr between the on-top and the fcc-hollow impact sites for $E_{\rm kin}^{\rm init} = 2$, 10, and 50 eV amounts to 0.55, 0.61, and 0.45 eV, respectively (see Fig. 7).

It has been discussed in the literature, by, e.g., Winter [15] or Krasheninnikov *et al.* [54] that after the charge transfer, an ionic projectile behaves just like an initially neutral one. In our TDDFT-MD simulations we observe small differences in the time development of the kinetic energy. Largest deviations occur in case of a proton impinging on the hollow site, which, however, are only of a similar size as the cluster size convergence effect presented in Sec. II. When the hydrogen is propagating inside the bulk material, differences in the time development of the kinetic energy of ≈250 meV are observed. The reason for this is not yet clear; it might be due to both the additional electron in case of the H^0-Al-cluster simulation as well as the H^+-ionization energy deposited in the Al cluster in case of the simulation with H^+ incident on the cluster.

F. Extrapolation from the cluster to the extended surface

We extrapolate our results from the Al cluster used in the simulation to the infinite Al(111) surface. Differences arise for two reasons: (i) In the simulation, the projectile starts at a finite separation $z_{\rm init} = 16$ bohr in front of the Al(111) facet of the cluster instead of an initially arbitrary large separation. (ii) In case of large H^+-Al_n separation, the image force acting on the H^+ is different for the finite-size cluster (where an image dipole is generated) and the metallic half space (where an image charge builds up).

In Sec. III C, we have argued that for H^+-Al_n distances $z <$ 8 bohr the results of the Al-cluster simulations can be used to describe the interaction between H^+ and the extended Al(111) surface. Furthermore, at a separation of H^+ from the Al(111) surface of $z = 8$ bohr, the $\bar{p}$-Al_n and the H^+-Al_n interaction potentials shown in Fig. 1 deviate by only 54 meV from each other, which corroborates the assumption that at separations $z > 8$ bohr the interaction between the proton and the metal surface is sufficiently well described by the image potential [55],

$$E_{\rm image}(z) = -\frac{1}{4(z - z_{\rm image})}, \tag{7}$$

as nonlinearities appear to be small (as derived from the cluster calculation, which, however, has a different asymptotic behavior). For the position $z_{\rm image}$ of the image plane in front of the Al(111) layer we use the value $z_{\rm image} = 3.14$ bohr obtained by Lam and Needs [56] within self-consistent pseudopotential-based density-functional calculations. Values for $z_{\rm image}$ have been discussed in the literature by Chulkov *et al.* in Ref. [57] where they have pointed out a variation of ±0.6 bohr depending on the calculation method. If $z_{\rm image}$ is allowed to vary by ±0.6 bohr, this would induce an uncertainty of $E_{\rm image}(z = 8\,\text{bohr})$ of ±0.2 eV. The kinetic energy of the projectile very far away from the surface, $E_{\rm kin}(z = \infty)$, is connected with the kinetic energy of the projectile at $z = 8$ bohr by energy conservation, i.e.:

$$E_{\rm kin}(z = \infty) = E_{\rm kin}(z = 8\,\text{bohr}) + E_{\rm image}(z = 8\,\text{bohr}). \tag{8}$$

We propagate the H^+ projectile from $z = 16$ bohr towards the surface and use the value of kinetic energy at $z = 8$ bohr in order to extrapolate to the kinetic energy of the proton at $z = \infty$ impinging on an infinite surface. We then let it propagate to the adsorption position of the H atom on the Born-Oppenheimer surface $z_{\rm ads}$ (which is significantly closer to the bulk than the neutralization position). As a last step we perform TDDFT-MD simulations with a neutral, spin-polarized H^0 atom and try to find the initial kinetic energy that leads to the same kinetic energy at the adsorption position as in the simulations with an H^+ projectile. The corresponding values for the kinetic energy are presented in Table I.

Specifically, for an H^+ impinging on the hollow site with a kinetic energy of the proton at $z = 16$ bohr of $E_{\rm kin}^{\rm init} = 2$ eV (first two rows of Table I, which actually refer to the same TDDFT-MD simulation) the extrapolation to the infinite surface yields $E_{\rm kin}(z = \infty) = 1.36$ eV. The kinetic energy of this projectile at the adsorption position (last column of Table I) is 4.03 eV and can also be obtained from a neutral H^0 projectile with an initial kinetic energy of 2.31 eV. The difference Δ between kinetic energy of H^+ and H^0 at $z = \infty$ amounts in this case to Δ ≈ 1.0 eV, denoted as Δ in Table I. In agreement with Ref. [51] we observe that in case of the H^0 projectile electronic friction effects start being relevant for $z < 8$ bohr. For this reason we assume here that $E_{\rm kin}^{\rm H^0}(z = \infty) \approx E_{\rm kin}^{\rm H^0}(z =$ 8 bohr).

Under the assumption of Sec. III E that after neutralization both projectiles behave the same, Table I draws an interesting picture about the initial kinetic energies resulting in the same kinetic energy of the projectile within the Al. For the lower kinetic energies of this study the initial kinetic energy far above the surface is for the H^+ projectile smaller than for

TABLE I. Kinetic energy of the H^+ or H^0 projectile (units of eV) approaching the Al cluster or Al(111) surface as a function of distance z from the plane of Al atoms. Simulations with H^0 are started from a ground-state simulation allowing for spin polarization. Impact points are fcc-hollow site or on-top site. Adsorption positions of H on Al(111) in ground-state calculation are $z_{\text{ads}}^{\text{hollow}} = 1.9$ bohr or $z_{\text{ads}}^{\text{top}} = 3.1$ bohr. Δ is the difference between the initial kinetic energies of H^+ and H^0 required to obtain identical velocities of the H^0 after scattering. [a]Extrapolation using Eq. (8); [b]value obtained from $E_{\text{kin}}(z=\infty) - E_{\text{image}}(z)$; [c]value taken from $z = 16$ bohr; [d]value taken from cluster simulation.

		$z=\infty$		$z = 16$ bohr	$z = 8$ bohr	$z = z_{\text{ads}}$
hollow	$H^+ \rightarrow$ Al cluster			2.00	2.76	4.03
	$H^+ \rightarrow$ Al surface	1.36[a]	$\Delta = +1.0$	1.89[b]	2.76[d]	4.03[d]
	$H^0 \rightarrow$ Al cluster	2.31[c]		2.31	2.31	4.03
hollow	$H^+ \rightarrow$ Al cluster			10.00	10.76	11.49
	$H^+ \rightarrow$ Al surface	9.36[a]	$\Delta = +0.6$	9.89[b]	10.76[d]	11.49[d]
	$H^0 \rightarrow$ Al cluster	9.95[c]		9.95	9.95	11.48
hollow	$H^+ \rightarrow$ Al cluster			50.00	50.76	49.86
	$H^+ \rightarrow$ Al surface	49.36[a]	$\Delta = -0.4$	49.89[b]	50.76[d]	49.86[d]
	$H^0 \rightarrow$ Al cluster	48.92[c]		48.92	48.92	49.88
top	$H^+ \rightarrow$ Al cluster			2.00	2.76	3.72
	$H^+ \rightarrow$ Al surface	1.36[a]	$\Delta = +0.8$	1.89[b]	2.76[d]	3.72[d]
	$H^0 \rightarrow$ Al cluster	2.16[c]		2.16	2.16	3.76
top	$H^+ \rightarrow$ Al cluster			10.00	10.76	10.92
	$H^+ \rightarrow$ Al surface	9.36[a]	$\Delta = +0.1$	9.89[b]	10.76[d]	10.92[d]
	$H^0 \rightarrow$ Al cluster	9.47[c]		9.47	9.47	10.91
top	$H^+ \rightarrow$ Al cluster			50.00	50.76	49.16
	$H^+ \rightarrow$ Al surface	49.36[a]	$\Delta = -1.2$	49.89[b]	50.76[d]	49.16[d]
	$H^0 \rightarrow$ Al cluster	48.15[c]		48.15	48.15	49.11

the H^0 projectile, i.e., $E_{\text{kin}}^{H^+}(z=\infty) < E_{\text{kin}}^{H^0}(z=\infty)$ whereas for the higher kinetic energies this relation inverts to $E_{\text{kin}}^{H^+}(z=\infty) > E_{\text{kin}}^{H^0}(z=\infty)$. Results are consistent with Fig. 6, i.e., a change of sign is also expected from the energy difference between the H^+-Al(111) interaction potential and the ground-state potential energy surface of H^0 in front of the Al(111) surface in the neutralization region.

G. Energy transfer from central collision

In order to draw a complete picture of the energy transfer, the energy dissipation into phononic degrees of freedom has to be calculated. Therefore, we perform TDDFT-MD simulations for the previously discussed Al_{188} cluster with H^+ initially located $z = 16$ bohr above the Al atoms. Thirteen Al atoms closest to the the impact point (impact at on-top site) were allowed to move in order to include the kinetic energy transfer into the substrate ionic degrees of freedom; the kinetic energy of the projectile is denoted as $E_{\text{kin}}^{\text{free}}$. Table II shows the difference in kinetic energy $(E_{\text{kin}}^{\text{free}} - E_{\text{kin}}^{\text{fix}})|_{z_{\text{exit}}}$ at the exit position $z_{\text{exit}} = 8$ bohr. $E_{\text{kin}}^{\text{fix}}$ refers to the kinetic energy of the projectile impinging on the Al cluster with frozen-in Al atomic coordinates.

TABLE II. Comparison of kinetic energies of H^+ projectiles incident on the Al(111) on-top site in case of frozen-in Al coordinates ($E_{\text{kin}}^{\text{fix}}$) and non-frozen-in Al coordinates ($E_{\text{kin}}^{\text{free}}$) when the projectile has reached $z_{\text{exit}} = 8$ bohr. For comparison, ΔE_{CC} denotes the kinetic energy transfer into the substrate in a head-on collision between an H atom and an Al atom [see Eq. (9)].

$E_{\text{kin}}^{\text{init}}$/eV	$(E_{\text{kin}}^{\text{free}} - E_{\text{kin}}^{\text{fix}})\|_{z_{\text{exit}}}$/eV	ΔE_{CC}/eV
2	−0.28	−0.14
10	−1.21	−1.39
50	−6.51	−6.95

The kinetic energy difference ranges from −0.28 eV for $E_{\text{kin}}^{\text{init}} = 2$ eV to −6.51 eV for $E_{\text{kin}}^{\text{init}} = 50$ eV. A semiquantitative understanding can be obtained from studying a simple central collision between a proton of mass m_{H} and an aluminum atom of mass m_{Al}. The kinetic energy transfer in a central collision is given by

$$\Delta E_{\text{CC}} = -\frac{4 m_{\text{H}} m_{\text{Al}}}{(m_{\text{H}} + m_{\text{Al}})^2} E_{\text{kin}}^{z=\infty} \approx -0.139 E_{\text{kin}}^{z=\infty}, \quad (9)$$

This results in an expected energy transfer of −0.14 eV for $E_{\text{kin}}^{\text{init}} = 2$ eV to −6.95 eV for $E_{\text{kin}}^{\text{init}} = 50$ eV.

The kinetic energy transfer into the phononic degrees of freedom during the central collision is small compared to the initial kinetic energy due to the significant mass difference between H and Al. For $E_{\text{kin}} \leqslant 10$ eV this brings the energy transfer caused by the image potential effects—which we discussed in the previous chapters—into the same order of magnitude.

IV. SUMMARY

We have performed TDDFT-MD simulations for the neutralization of hyperthermal H^+ projectiles impinging on an Al(111) surface, which is modeled by a finite-size cluster. It has been remarked by Winter *et al.* [15] that the neutralization distance may be derived from a comparison of scattered ionic and neutral projectiles. Following these ideas, we have

simulated the process from *ab initio* and calculated the scattering of H^+ and H^0 projectiles for two different impact sites. By this means we have been able to link the charge transfer with the electronic energy transfer due to neutralization.

In case of the projectiles studied here with a kinetic energy ranging between 2 and 50 eV, the maximum of the neutralization rate occurs in a region between $z = 4.2$ bohr and $z = 5.1$ bohr in front of the uppermost Al atom layer, independent of impact site. Additionally, we find that, in order to obtain identical exit velocities in case of projectiles with $E_{\mathrm{kin}} \approx 50$ eV, H^+ needs to be initially faster than H^0 by about 1.2 eV (on-top trajectory) to 0.4 eV (fcc-hollow trajectory). In contrast, for projectiles with $E_{\mathrm{kin}} \approx 2$ eV the sign changes and H^+ needs to be initially slower than H^0 by about 0.8 eV (on-top trajectory) to 1.0 eV (fcc-hollow trajectory). This is explained by the difference between the ground-state potential energy surface and the H^+-Al(111) interaction potential which is repulsive in the region of neutralization.

ACKNOWLEDGMENTS

We thank A. C. Dávila López for helpful discussions. Calculations were carried out at the Rechenzentrum der Universität Kiel.

[1] I. Adamovich, S. D. Baalrud, A. Bogaerts, P. J. Bruggeman, M. Cappelli, V. Colombo, U. Czarnetzki, U. Ebert, J. G. Eden, P. Favia, D. B. Graves, S. Hamaguchi, G. Hieftje, M. Hori, I. D. Kaganovich, U. Kortshagen, M. J. Kushner, N. J. Mason, S. Mazouffre, S. M. Thagard *et al.*, J. Phys. D **50**, 323001 (2017).

[2] M. Bonitz, A. Filinov, J.-W. Abraham, K. Balzer, H. Kählert, E. Pehlke, F. X. Bronold, M. Pamperin, M. Becker, D. Loffhagen, and H. Fehske, Frontiers Chem. Sci. Eng. **13**, 201 (2019).

[3] D. M. Newns, Phys. Rev. **178**, 1123 (1969).

[4] R. Brako and D. Newns, Surf. Sci. **108**, 253 (1981).

[5] J. Geerlings, J. Los, J. Gauyacq, and N. Temme, Surf. Sci. **172**, 257 (1986).

[6] J. Merino, N. Lorente, P. Pou, and F. Flores, Phys. Rev. B **54**, 10959 (1996).

[7] D. C. Langreth and P. Nordlander, Phys. Rev. B **43**, 2541 (1991).

[8] M. Pamperin, F. X. Bronold, and H. Fehske, Phys. Rev. B **91**, 035440 (2015).

[9] M. Bonitz, K. Balzer, N. Schlünzen, M. R. Rasmussen, and J. Joost, Phys. Status Solidi (b) **256**, 1970028 (2019).

[10] M. A. L. Marques, C. A. Ullrich, F. Nogueira, A. Rubio, K. Burke, and E. K. U. Gross, editors, *Time-Dependent Density Functional Theory*, Lecture Notes in Physics Vol. 706 (Springer, Berlin/Heidelberg, 2006).

[11] M. A. L. Marques, N. T. Maitra, F. M. S. Nogueira, E. K. U. Gross, and A. Rubio, editors, *Fundamentals of Time-Dependent Density Functional Theory*, Lecture Notes in Physics Vol. 837 (Springer, Berlin/Heidelberg, 2012).

[12] M. A. Marques, A. Castro, G. F. Bertsch, and A. Rubio, Comput. Phys. Commun. **151**, 60 (2003).

[13] R. Baragiola, E. Alonso, J. Ferron, and A. Oliva-Florio, Surf. Sci. **90**, 240 (1979).

[14] D. Hasselkamp, S. Hippler, and A. Scharmann, Nucl. Instrum. Methods Phys. Res. B **18**, 561 (1986).

[15] H. Winter, J. Phys.: Condens. Matter **8**, 10149 (1996).

[16] H. Winter and A. Borisov, Nucl. Instrum. Methods Phys. Res. B **115**, 211 (1996).

[17] H. Nienhaus, R. Zimny, and H. Winter, Radiat. Eff. Defects Solids **109**, 1 (1989).

[18] A. Borisov and H. Winter, Nucl. Instrum. Methods Phys. Res. B **115**, 142 (1996).

[19] M. Okada and Y. Murata, J. Phys.: Condens. Matter **9**, 1919 (1997).

[20] W. Heiland, Surf. Sci. **251-252**, 942 (1991).

[21] H. Eder, F. Aumayr, P. Berlinger, H. Störi, and H. Winter, Surf. Sci. **472**, 195 (2001).

[22] P. Nordlander and J. C. Tully, Phys. Rev. B **42**, 5564 (1990).

[23] P. Nordlander and J. C. Tully, Phys. Rev. Lett. **61**, 990 (1988).

[24] S. A. Deutscher, X. Yang, and J. Burgdörfer, Phys. Rev. A **55**, 466 (1997).

[25] J. Merino, N. Lorente, M. Y. Gusev, F. Flores, M. Maazouz, L. Guillemot, and V. A. Esaulov, Phys. Rev. B **57**, 1947 (1998).

[26] A. Borisov, D. Teillet-Billy, and J. Gauyacq, Nucl. Instrum. Methods Phys. Res. B **78**, 49 (1993).

[27] M. C. Torralba, P. G. Bolcatto, and E. C. Goldberg, Phys. Rev. B **68**, 075406 (2003).

[28] R. Monreal and F. Flores, in *Theory of the Interaction of Swift Ions with Matter. Part 1*, Advances in Quantum Chemistry Vol. 45 (Academic Press, Cambridge, 2004), pp. 175–199.

[29] K. Snowdon, R. Hentschke, A. Närmann, W. Heiland, E. Mühling, and W. Eckstein, Nucl. Instrum. Methods Phys. Res. B **23**, 309 (1987).

[30] B. Obreshkov and U. Thumm, Phys. Rev. A **87**, 022903 (2013).

[31] H. Jouin and F. A. Gutierrez, Phys. Rev. A **80**, 042901 (2009).

[32] H. Jouin and F. A. Gutierrez, Phys. Rev. A **84**, 014901 (2011).

[33] J. Juaristi, Nucl. Instrum. Methods Phys. Res. B **230**, 148 (2005), Atomic Collisions in Solids.

[34] N. Schlünzen, K. Balzer, M. Bonitz, L. Deuchler, and E. Pehlke, Contrib. Plasma Phys. **59**, e201800184 (2019).

[35] Please note that the image plane position of an Al(111) surface is located approximately 3.14 bohr in front of the uppermost Al atom; see Ref. [56].

[36] K. A. H. German, C. B. Weare, and J. A. Yarmoff, Phys. Rev. B **50**, 14452 (1994).

[37] A. Castro, H. Appel, M. Oliveira, C. A. Rozzi, X. Andrade, F. Lorenzen, M. A. L. Marques, E. K. U. Gross, and A. Rubio, physica status solidi (b) **243**, 2465 (2006).

[38] X. Andrade, D. Strubbe, U. De Giovannini, A. H. Larsen, M. J. T. Oliveira, J. Alberdi-Rodriguez, A. Varas, I. Theophilou, N. Helbig, M. J. Verstraete, L. Stella, F. Nogueira, A. Aspuru-Guzik, A. Castro, M. A. L. Marques, and A. Rubio, Phys. Chem. Chem. Phys. **17**, 31371 (2015).

[39] J. P. Perdew, K. Burke, and M. Ernzerhof, Phys. Rev. Lett. **77**, 3865 (1996).

[40] N. Troullier and J. L. Martins, Phys. Rev. B **43**, 1993 (1991).
[41] M. Fuchs and M. Scheffler, Comput. Phys. Commun. **119**, 67 (1999).
[42] C. A. Rozzi, D. Varsano, A. Marini, E. K. U. Gross, and A. Rubio, Phys. Rev. B **73**, 205119 (2006).
[43] M. Tafipolsky and R. Schmid, J. Chem. Phys. **124**, 174102 (2006).
[44] M. Methfessel and A. T. Paxton, Phys. Rev. B **40**, 3616 (1989).
[45] D. Marx and J. Hutter, *Ab Initio Molecular Dynamics: Basic Theory and Advanced Methods* (Cambridge University Press, Cambridge, 2009).
[46] A. Liebsch, Phys. Rev. B **36**, 7378 (1987).
[47] S. Andersson and B. N. J. Persson, Phys. Rev. Lett. **50**, 2028 (1983).
[48] A. Gras-Marti, P. Echenique, and R. Ritchie, Surf. Sci. **173**, 310 (1986).
[49] W. Tang, E. Sanville, and G. Henkelman, J. Phys.: Condens. Matter **21**, 084204 (2009).
[50] A. Kiejna and B. I. Lundqvist, Phys. Rev. B **63**, 085405 (2001).
[51] M. Lindenblatt, E. Pehlke, A. Duvenbeck, B. Rethfeld, and A. Wucher, Nucl. Instrum. Methods Phys. Res. B **246**, 333 (2006).
[52] M. Alducin, R. D. Muiño, and J. I. Juaristi, Prog. Surf. Sci. **92**, 317 (2017).
[53] M. Lindenblatt and E. Pehlke, Phys. Rev. Lett. **97**, 216101 (2006).
[54] A. V. Krasheninnikov, Y. Miyamoto, and D. Tománek, Phys. Rev. Lett. **99**, 016104 (2007).
[55] N. D. Lang and W. Kohn, Phys. Rev. B **7**, 3541 (1973).
[56] S. C. Lam and R. J. Needs, J. Phys.: Condens. Matter **5**, 2101 (1993).
[57] E. Chulkov, V. Silkin, and P. Echenique, Surf. Sci. **437**, 330 (1999).